Effect of hydrogen concentration and strain rate on hydrogen embrittlement of ultra-fine grained low carbon steel

E.D. Merson - Institute of Advanced Technologies, Togliatti State University, Belorusskaya str. 14, Togliatti 445667, Russian Federation, Mersoned@gmail.com

P.N. Myagkikh - Institute of Advanced Technologies, Togliatti State University, Belorusskaya str. 14, Togliatti 445667, Russian Federation, feanorhao@gmail.com

G.V. Klevtsov - Institute of Advanced Technologies, Togliatti State University, Belorusskaya str. 14, Togliatti 445667, Russian Federation, klevtsov11948@mail.ru

D. Merson - Institute of Advanced Technologies, Togliatti State University, Belorusskaya str. 14, Togliatti 445667, Russian Federation, d.merson@tltsu.ru

A. Vinogradov - Department of Mechanical and Industrial Engineering, Norwegian University of Science and Technology – NTNU, N-7491 Trondheim, Norway, alexei.vino@gmail.com

Abstract

During the last few decades, keen attention has been paid to the advanced steels with the ultra-fine grained (UFG) microstructure manufactured by severe plastic deformation (SPD) techniques. Although these materials often demonstrate prominent mechanical properties, the detrimental environmentally-induced effects, such as hydrogen embrittlement (HE), which may appear during their service life, have been just scarcely studied. In particular, the influence of the hydrogen concentration and strain rate, which are among the main factors controlling HE, in general, has not been considered in UFG ferritic steels as yet. Thus, the objective of the present study was to examine the effect of these factors on the mechanical behav-

iour and fracture mode of the low-alloy steel processed by ECAP in comparison with the conventionally fabricated counterparts. The ECAPed and as-received specimens of the low-alloy steel grade 09G2S were cathodically hydrogen charged at different current densities and then subjected to tensile testing at two different strain rates. The diffusible hydrogen concentration in the specimens before tensile testing was assessed by the hot-extraction method. After hydrogen charging both as-received and ECAPed specimens demonstrate HE the extent of which increases with the increasing hydrogen concentration and decreasing strain rate. It is found that the ECAPed steel occludes much higher hydrogen concentration than the as-received one. At the given hydrogen concentration, the ECAPed specimens demonstrate stronger hydrogen-induced ductility loss as well as the fundamentally different fracture mode in comparison to the as-received counterparts.

1. Introduction

Grain refinement is the one of the most effective methods for strength enhancement in metals, which can be achieved without significant compromising ductility and fracture toughness [1,2]. Severe plastic deformation (SPD) techniques, among which are equal-channel angular pressing (ECAP), high-pressure torsion (HPT) and many others, have been devised to provide extreme grain size reduction down to the sub-micrometre scale in many bulk metallic materials including Al [3], Ti [4], Mg [5], Fe-based alloys [6–8], etc. The ultra-fine grained (UFG) materials obtained in this way demonstrate tremendous strength and ductility balance due to which they received keen attention from material scientists and engineers during the past few decades [9,10]. In particular, substantial efforts have been made to use the SPD methods for improvement of mechanical properties of low-carbon and low-alloy steels [7,11,12]. While the strength of these materials processed by conventional heat-treatment is limited to 600-650 MPa, the SPD techniques can provide the increase of the ultimate tensile strength of low-carbon iron up to 1500 MPa which is a very remarkable result [12]. Besides the mechanical properties, the critical factor determining the service performance of structural steels is their resistance to environmentally-induced effects such as corrosion, stress-corrosion cracking and hydrogen embrittlement (HE). The latter is a well-known phenomenon referred to the deterioration of ductility and other mechanical properties of metals caused by hydrogen, which dissolves and diffuses easily in metals during service life. Fundamental mechanisms of HE are considered and discussed elsewhere in great details [13,14]. The high-strength steels demonstrate a much higher susceptibility to HE than the mild steels. Therefore, the effect of

hydrogen on UFG steels is of substantial practical concern. Although some limited data on HE of the UFG steels can be found in the literature [8,12,15,16], many important issues related to this phenomenon have been not considered as yet. For example, the effect of hydrogen concentration and strain rate, which are best known among the main factors controlling the HE extent, has not been quantified and reported for UFG ferritic steels. Thus, the main objective of the present study was to examine the effect of hydrogen concentration and strain rate on HE of the low-alloy steel with the UFG microstructure processed by ECAP.

2. Experimental

The hot-rolled bars of commercial low-alloy steel grade 09G2S with the chemical composition represented in Table 1 were subjected to the thermo-mechanical treatment including the following steps: (i) homogenising annealing at 810 °C followed by quenching in water, (2) tempering at 450 °C, (3) cold severe plastic deformation by the "CONFORM" ECAP (equal channel angular pressing) [17] process to 4 passes by the Bc route and (4) annealing at 350 °C for residual stress removing. Using the electric discharge machine, the as-received and ECAPed bars were longitudinally sliced into 2 mm thick plates from which the specimens for tensile testing with the 4×15 mm^2 gauge part as well as small rectangular specimens for gas analysis with 4×20 mm^2 dimensions were cut out. The surface of all samples was grounded with emery paper to the #240 grade.

Table 1. Chemical composition of the steel grade 09G2S, w. %

C	Si	Mn	P	S	Cr	Ni	Cu	V	Al	Fe
0.091	0.722	1.358	0.016	0.011	0.097	0.072	0.235	<0.005	0.018	Base

The specimens were cathodically hydrogen charged in the 5% H2SO4 + 1.5 g/l thiourea solution with the platinum wire used as an anode. To vary the hydrogen concentration, the current density was ranged from 0.3 to 400 mA/cm^2 while the charging time of 1 hour was the same in all tests. Within 5 minutes after hydrogen charging, the specimens were washed with running water and CCl4 and then subjected to the gas-analysis or mechanical testing.

Mechanical testing has been conducted using the screw-driven N50KT (Tinius Olsen) testing machine. Two different nominal strain rates of $5 \cdot 10^{-3}$ and $5 \cdot 10^{-2}$ s^{-1} were used (the corresponding traverse velocities were of 5 mm/min and 50 mm/min). After the tensile test, one half of the specimen was subjected to the gas-analysis to assess the residual hydrogen concentration, while the other half was used for fractographic observations.

The gas-analysis was performed by the hot-extraction method using the Galileo G8 (Bruker) gas-analyser. To analyse the diffusible hydrogen concentration in steel, each specimen was inserted in the quarts tube of the gas-analyser where it was heated up to 200 °C in N_2 gas flux with the heating rate of 17 °C/min and held at the destination temperature for 15 min.

The fractographic and metallographic examinations have been conducted using the scanning electron microscope (SEM) SIGMA (ZEISS) equipped with the electron backscattering diffraction (EBSD) facilities.

3. Results and discussion

3.1. Microstructure

In the as-received state, the steel has a typical ferrite-pearlite microstructure represented by equiaxed coarse grains of 10 μm average diameter, Fig. 1a. The wide assortment of non-metallic inclusions such as MnS is also observed in the microstructure, see the inset in Fig. 1a. As can be seen on SEM images presented in Fig. 1b, the ECAP results in distortion of the grain boundaries as well as in the stretching of the initial grains in the shear direction at 45° to the extrusion direction. The stretching is more severe at the peripheral part of the ECAPed bar. When examined by the EBSD technique, the microstructure of the ECAPed steel reveals small grains and sub-grains separated by dislocation boundaries, see Fig. 1c. The average grain size of the ECAPed steel assessed by EBSD for the grains separated by high angle boundaries with misorientation angles exceeding 15° is of 0.6 μm.

After hydrogen charging, both kinds of specimens exhibit hydrogen-induced defects in the microstructure and on the surface, c.f. Fig. 1d-f. Hydrogen-induced cracks (HICs) and blisters (HIBs) are present in the microstructure and on the surface of the as-received specimens, respectively, Fig. 1d, e. HICs are primarily transgranular, Fig. 1d, although some intergranular ones are also can be found, Fig. 2e. The number and size of HICs and HIBs in the as-received steel grow with the increasing current density of hydrogen charging. The ECAPed specimens surface reveals no HIBs, yet the HICs, which occasionally connected with the specimen's surface, are readily observed in the microstructure, see Fig. 1f. Most of the HICs of the ECAPed steel have the same orientation, which coincides with the grains stretching direction caused by the ECAP simple shear process. These HICs are transgranular with respect to the initial ferritic grains. However, they likely can propagate along the dislocation sub-grains boundaries.
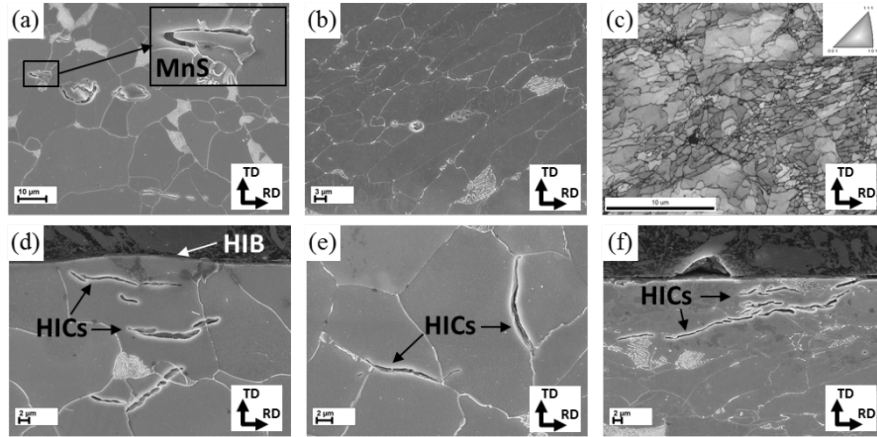
Fig. 1. SEM images (a, b, d-f) and inverse pole figure (IPF) colored orientation map obtained by EBSD from the microstructure of the as-received (a, d, e) and the ECAPed (b, c, f) specimens of the low-alloy steel grade 09G2S before (a-c) and after (d-f) cathodic hydrogen charging

3.2. Gas-analysis

The gas-analysis showed that diffusible hydrogen is absent in the uncharged specimens of both kinds. As can be seen in the histogram in Fig. 2, the concentration of diffusible hydrogen in the charged specimens increases with the increasing current density. At given charging conditions, the ECAPed steel occludes much higher hydrogen concentration than its as-received counterpart, that is obviously due to the substantially higher density of dislocations and grain boundaries acting as hydrogen traps. One can notice that the significant increase in the hydrogen concentration in the ECAPed steels occurs at the current densities below 20 mA/cm2, while the further growth of current density up to 400 mA/cm2 does not affect the hydrogen content considerably. In contrast, the hydrogen concentration in the as-received steel grows significantly as the current density increases from 20 to 400 mA/cm2. The effect of current density on the hydrogen concentration and hydrogen-induced defects in the same materials has been considered in the dedicated paper in detail [16]. It was shown in particular that the increase of the hydrogen concentration in the as-received steel in the current density range of 20-400 mA/cm2 is associated with intensive blistering that does not occur in the UFG steel obtained by ECAP.
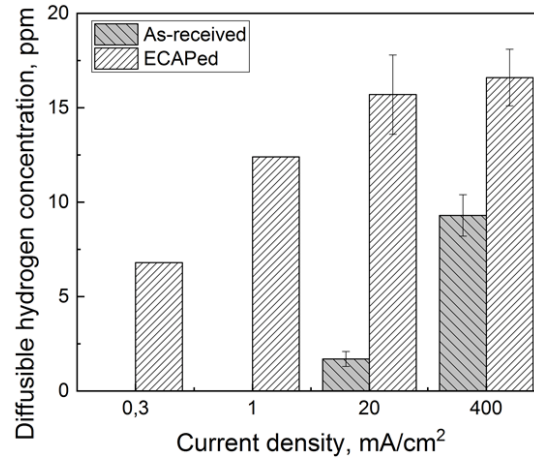
Fig. 2. Effect of cathodic hydrogen charging current density on the diffusible hydrogen concentration in the as-received and ECAPed low-alloy steel 09G2S.

3.3. Mechanical testing

The results of the tensile tests showed that the hydrogen-free as-received specimens demonstrate significant elongation to failure and moderate strength. The pronounced yield plateau, strain hardening and necking regions are evident on the stress-strain diagrams of these specimens at low and high strain rates as can be seen in Fig. 3. After ECAP, the ultimate tensile strength (UTS) of the steel increases from 485 up to 840 MPa, while the elongation compromises from 40 down to 15%. Besides, the yield plateau vanishes and the strain hardening region becomes hardly visible on the stress-strain diagrams. The increase of the strain rate expectedly provides a slight increase in strength and the decrease in elongation to failure of both as-received and ECAPed specimens.

Hydrogen charging results in substantial ductility drop for the specimens of both kinds. As can be seen in Fig. 4a and b, the hydrogen-induced ductility loss of the as-received and ECAPed specimens increases with the increasing hydrogen concentration and decreasing strain rate. At all conditions, the ECAPed specimens show the much more significant ductility loss due to HE than their as-received counterparts. Regardless of the hydrogen concentration and strain rate, the hydrogen charged conventional specimens always fracture after notable yielding, strain-hardening and necking while the ECAPed specimens brake at the stress below the yield point, Fig. 3. That is why the hydrogen charging results in the significant drop of UTS in the ECAPed steel, while the UTS of the as-received specimens even slightly increases as the hydrogen concentration increases, c.f. Fig. 4c. For the same reason, the effect of hydrogen concentration on HE of the ECAPed steel

is better evaluated by the change in UTS than by elongation or associated ductility loss, which are more informative about the severity of HE in the as-received steel.
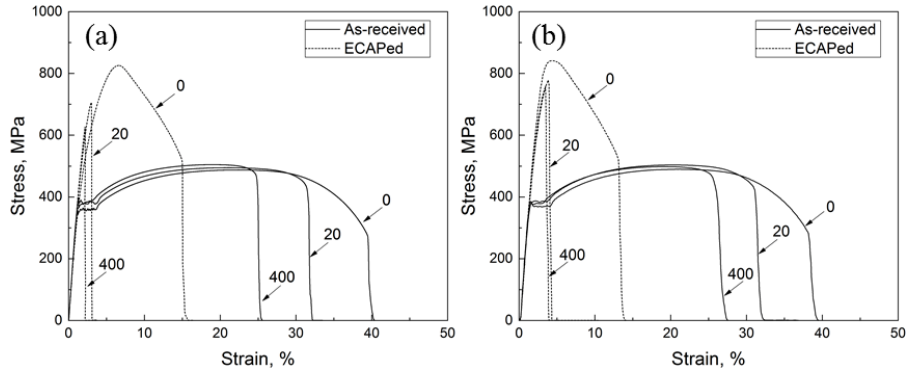

Fig. 3. Stress-strain diagrams of the as-received and ECAPed specimens before and after hydrogen charging at low (a) and high (b) strain rate.
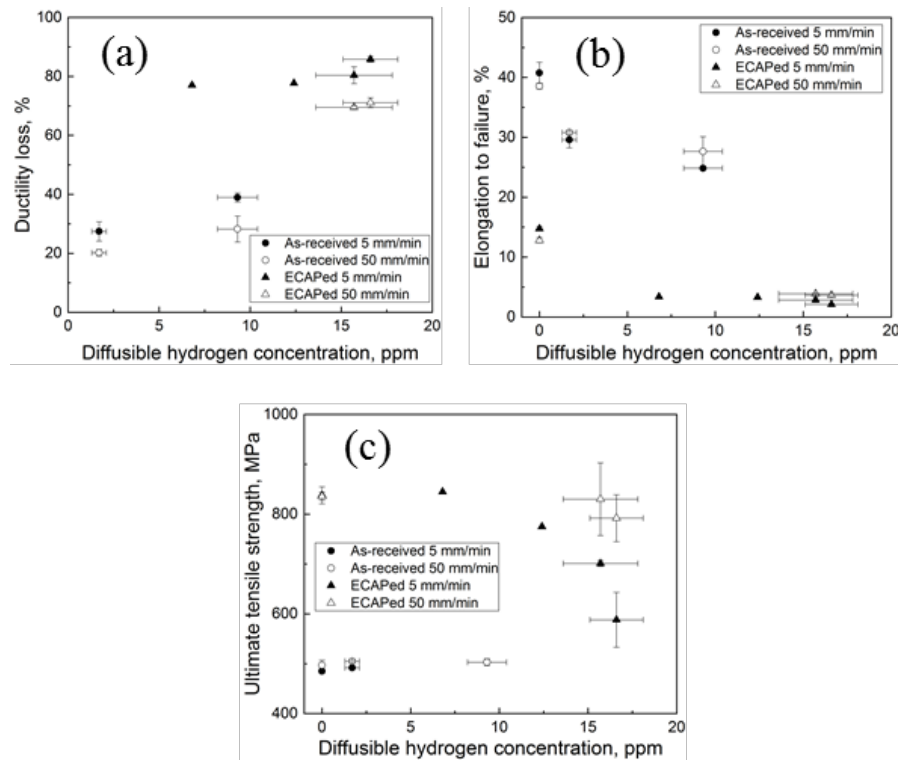

Fig. 4. Effect of the diffusible hydrogen concentration on the ductility loss (a), elongation to failure (b) and ultimate tensile strength (c) of the as-received and ECAPed specimens at low and high strain rate of tensile testing.

3.4. Fractography

The hydrogen-free specimens in the as-received and ECAPed states after tensile testing have completely ductile fracture surface with dimples nucleated at non-metallic inclusions and pearlitic grains, Fig. 5a, b, 6a, b and 7a, b. The fracture surfaces of the hydrogen charged as-received specimens contain "fisheyes" – the round-shape areas with quasi-cleavage morphology and non-metallic inclusions in their centers, Fig. 5c-f and 7c, d. Depending on the current density and strain rate, the total area of the fisheyes is about 40-50% of the fracture surface area, while the rest is represented by the ductile dimpled relief. Fisheyes are produced by the hydrogen-assisted growth of radial cracks nucleating at non-metallic inclusions. Details of the formation mechanism of these defects and the nature of the quasi-cleavage morphology have been considered elsewhere [8,18–21].
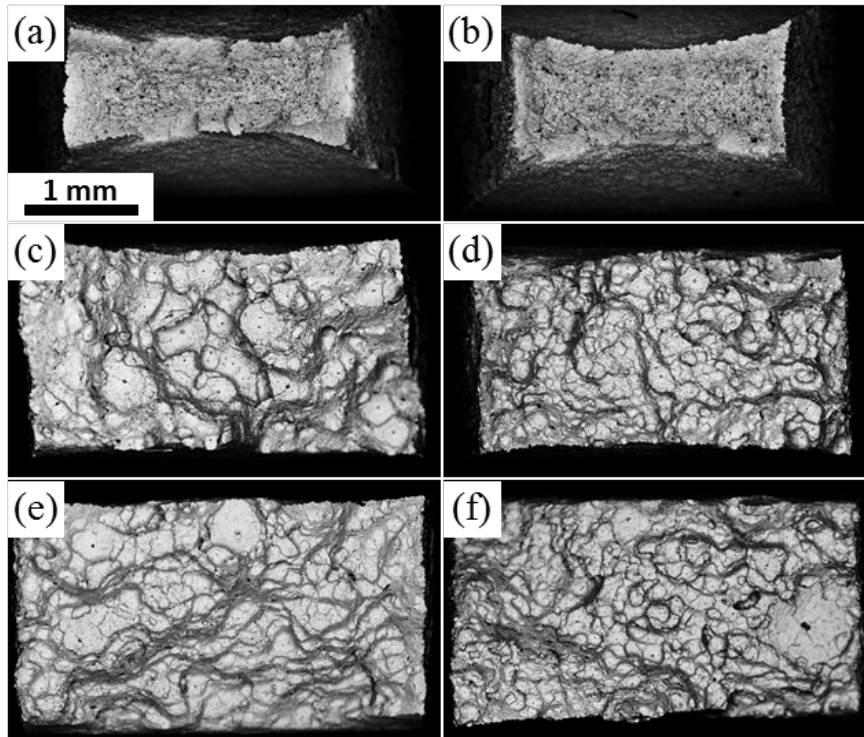

Fig. 5. Full-scale views of the fracture surfaces of the as-received specimens of the low-alloy steel grade 09G2S tested at 5 (a, c, e) and 50 mm/min (b, d, f) traverse velocity in the hydrogen free state (a, b) and after hydrogen charging at 20 (c, d) and 400 mA/cm^2 (e, f). Backscattering electron contrast images obtained by SEM.
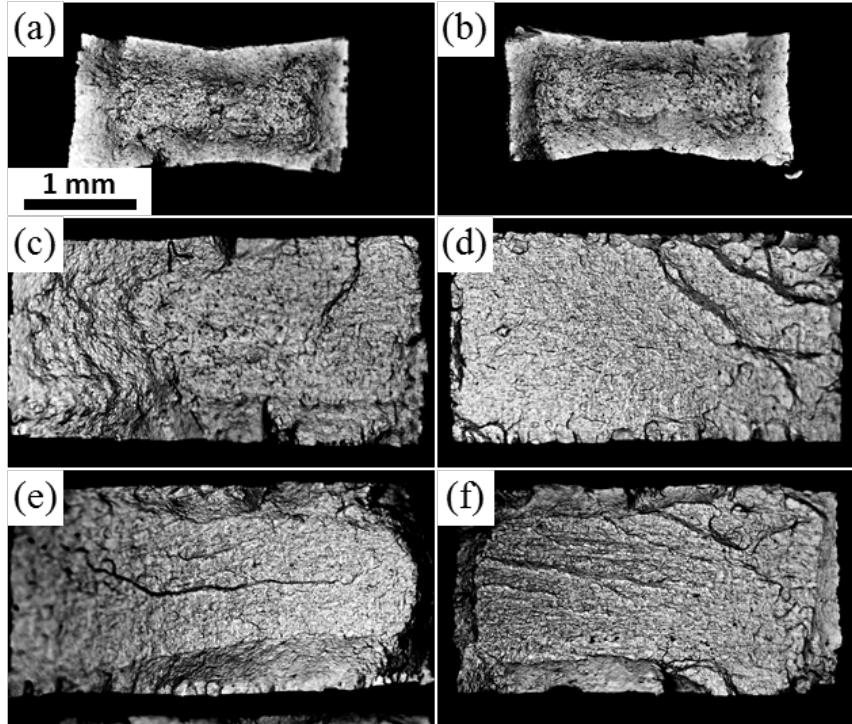
Fig. 6. Full-scale views of the fracture surfaces of the ECAPed specimens of the low-alloy steel grade 09G2S tested at 5 (a, c, e) and 50 mm/min (b, d, f) traverse velocity in the hydrogen free state (a, b) and after hydrogen charging at 20 (c, d) and 400 mA/cm^2 (e, f). Backscattering electron contrast images obtained by SEM.

The quantitative fractographic analysis showed that the increase of both the hydrogen concentration and the strain rate results in the growth of the number of fisheyes as well as in the reduction of their mean area and diameter, Fig. 5c-f and 8. It is known that the presence of hydrogen at stress risers such as non-metallic inclusions or HICs in steel is a prerequisite for the fisheyes formation [20]. As was shown above, hydrogen charging at the higher current density provides both the increased hydrogen concentration and the greater number of HICs. Since the HICs at the same time act as the points of high hydrogen and stress concentration, and, thus, as the favourable nucleation sights for the fisheyes cracks, the increase of the HICs number should cause the rise of the number of fisheyes. It is reasonable to suppose that during the tensile test, the fisheyes nucleate more readily at the sights with the highest stress and hydrogen concentration. Initiation and propagation of the fisheye crack provide the increase of triaxial stresses ahead of its tip. The regions with high triaxial stresses attract hydrogen, which can diffuse from the neighbouring areas. On the one hand, the supply of extra hydrogen to the crack tip maintains the propagation of this crack and, hence, the further increase of triaxial

stress which attracts more hydrogen. On the other hand, the consumption of hydrogen in the neighbouring areas restricts the nucleation of new fisheyes in those areas. However, when the strain rate is high, there is less time to hydrogen diffusion, while the stress increases quickly so that more fisheyes have a chance to initiate. The aforesaid provides a plausible explanation for the increase in the number of fisheyes and the decrease of their mean dimensions at the increasing strain rate as is observed in the present study.
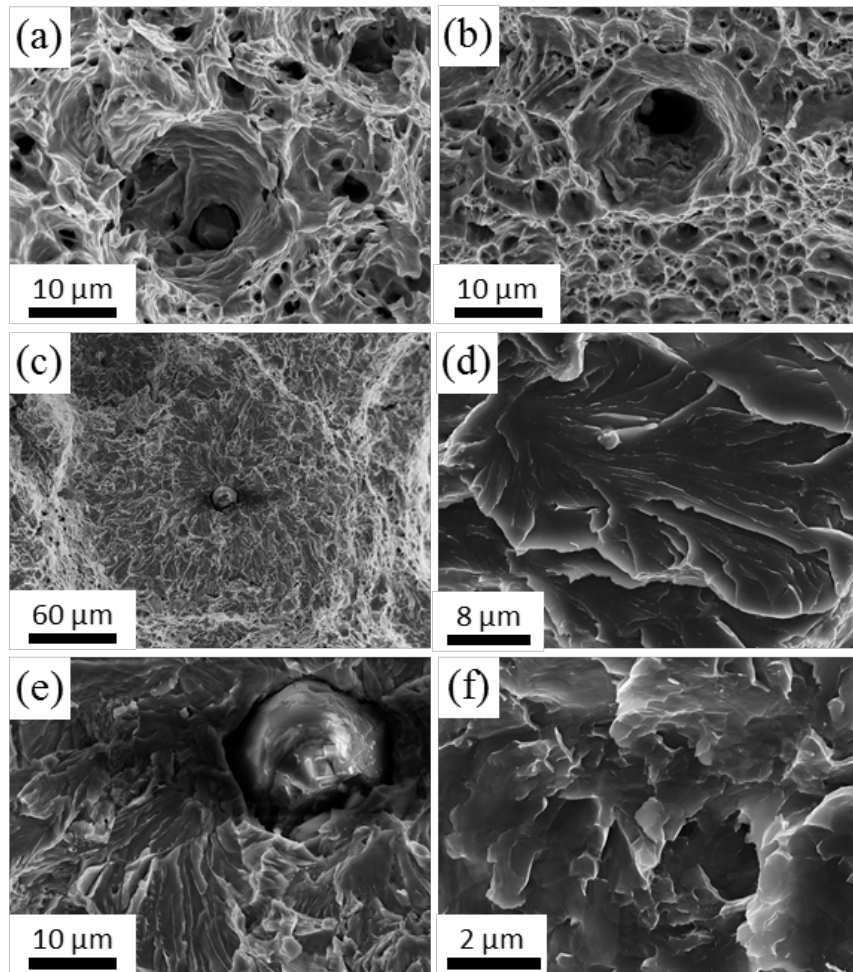

Fig. 7. SEM images demonstrating characteristic features of the fracture surfaces of the as-received (a-c) and ECAPed (d-f) specimens tested before (a, d) and after (b, c, e, f) hydrogen charging: (a, d) – dimpled relief, (b) – fisheye, (c) – fisheye's quasi-cleavage, (e) – true cleavage, (f) – tearing morphology.

Regardless of the hydrogen concentration and strain rate, the fracture surfaces of the hydrogen charged ECAPed steel are entirely brittle, Fig. 6c-f . In this case, the fracture surface is seen as a mixture of true cleavage, Fig. 7d, and specific tearing morphology, Fig. 7f , which is believed to be produced by the hydrogen-assisted cracking along dislocation boundaries of the UFG microstructure of the ECAPed steel [8]. Nevertheless, the exact formation mechanism of the tearing morphology is to be revealed.
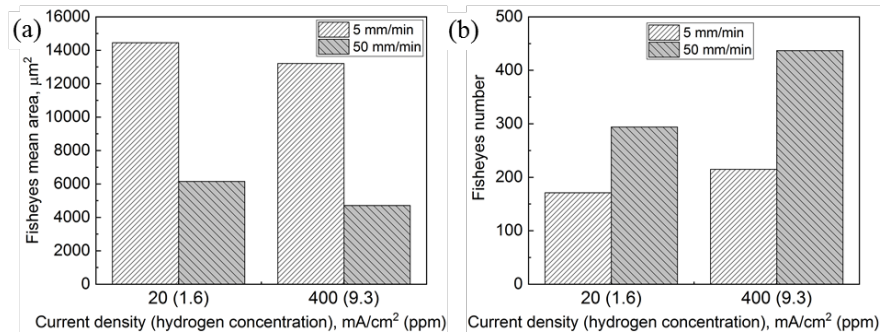

Fig. 8. Effect of cathodic hydrogen charging current density (diffusible hydrogen concentration) and strain rate on the mean area (a) and number (b) of fisheyes in the fracture surfaces of the hydrogen charged as-received specimens of the low-alloy steel grade 09G2S.

4. Summary and conclusions

It is shown in the present study that the microstructure refinement by the ECAP process provides substantial strengthening of the low-alloy steel grade 09G2S whereas the ductility and the susceptibility to HE is significantly compromised. Moreover, ECAP fundamentally changes the fracture mode of hydrogen-assisted cracking and strongly affects the HE features in the low-alloy steel. The main findings of the present study are as follows.

1. At given cathodic hydrogen charging conditions, the ECAPed steel occludes much higher hydrogen concentration than its as-received hot-rolled counterpart that is apparently due to the increased dislocation density and the volume fraction of grain boundaries serving as hydrogen traps.
2. At given hydrogen concentration and mechanical testing conditions, the ECAPed steel demonstrates more severe ductility loss than its conventional counterpart.
3. The hydrogen charged UFG low-carbon steel obtained by ECAP exhibits HE features which are inherent for the most of high-strength steels embrittled by hydrogen. Specifically, (i) it fractures in the quasi-elastic strain region of the stress-strain diagram, (ii) it shows an entirely brittle fracture surface, (iii) the

HE is enhanced at the increasing hydrogen concentration and decreasing strain rate (the latter is also common for other hydrogen embrittled steels and alloys).

4. The fracture surface of the hydrogen charged as-received low-alloy steel is composed of ductile dimpled relief and round-shaped quasi-cleavage regions – fisheyes, which number increases but mean area decreases with increasing hydrogen concentration and strain rate. The fracture surface of the hydrogen embrittled ECAPed steel does not contain fisheyes. However, it is wholly composed of true cleavage and tearing fracture morphology, which formation mechanism is still unknown and is to be revealed.

Acknowledgements

References

[1] R. Valiev, Nanostructuring of metals by severe plastic deformation for advanced properties, Nat. Mater. 3 (2004) 511–516. doi:10.1038/nmat1180.

[2] A. Azushima, R. Kopp, A. Korhonen, D.Y. Yang, F. Micari, G.D. Lahoti, et al., Severe plastic deformation (SPD) processes for metals, CIRP Ann. - Manuf. Technol. 57 (2008) 716–735. doi:10.1016/j.cirp.2008.09.005.

[3] E. Khafizova, R. Islamgaliev, G. Klevtsov, E. Merson, Microstructure, strength and fatigue of an ultrafine-grained Al-Cu-Mg alloy, Mater. Phys. Mech. 24 (2015) 232–241.

[4] I. Sabirov, R.Z. Valiev, I.P. Semenova, R. Pippan, Effect of Equal Channel Angular Pressing on the Fracture Behavior of Commercially Pure Titanium, Metall. Mater. Trans. A. 41 (2010) 727–733. doi:10.1007/s11661-009-0111-z.

[5] A. Vinogradov, V.N. Serebryany, S. V. Dobatkin, Tailoring microstructure and properties of fine grained magnesium alloys by severe plastic deformation, Adv. Eng. Mater. 20 (2018) 1–22. doi:10.1002/adem.201700785.

[6] A. Hohenwarter, R. Pippan, Fracture of ECAP-deformed iron and the role of extrinsic toughening mechanisms, Acta Mater. 61 (2013) 2973–2983. doi:http://dx.doi.org/10.1016/j.actamat.2013.01.057.

[7] S. Dobatkin, P.D. Odessky, S. V. Shagalina, Ultrafine Grained Low Carbon Steels Processed by Severe Plastic Deformation, Mater. Sci. Forum. 584–586 (2008) 623–630. doi:10.4028/www.scientific.net/MSF.584-586.623.

[8] E.D. Merson, P.N. Myagkikh, G.V. Klevtsov, D.L. Merson, A. Vinogradov, Effect of fracture mode on acoustic emission behavior in the hydrogen embrittled low-alloy steel, Eng. Fract. Mech. 210 (2019) 342–357. doi:10.1016/j.engfracmech.2018.05.026.

[9] Y. Estrin, A. Vinogradov, Extreme grain refinement by severe plastic deformation: A wealth of challenging science, Acta Mater. 61 (2013) 782–817. doi:10.1016/j.actamat.2012.10.038.

[10] A. Vinogradov, Mechanical Properties of Ultrafine-Grained Metals: New Challenges and Perspectives, Adv. Eng. Mater. 17 (2015) 1710–1722. doi:10.1002/adem.201500177.

[11] F. Soleimani, M. Kazeminezhad, Synergistic Strengthening by Severe Plastic Deformation and Post-Heat Treatment of a Low-Carbon Steel, Steel Res. Int. 89 (2018) 1–10. doi:10.1002/srin.201700548.

[12] Y. Mine, S. Matsumoto, Z. Horita, Strengthening and hydrogen embrittlement of ultrafine-grained Fe–0.01mass% C alloy processed by high-pressure torsion, Corros. Sci. 53 (2011) 2969–2977. doi:10.1016/j.corsci.2011.05.052.

[13] I.M. Robertson, P. Sofronis, A. Nagao, M.L. Martin, S. Wang, D.W. Gross, et al., Hydrogen Embrittlement Understood, Metall. Mater. Trans. A. 46 (2015) 2323–2341. doi:10.1007/s11661-015-2836-1.

[14] S.P. Lynch, Hydrogen embrittlement phenomena and mechanisms, Corros. Rev. 30 (2012) 63–133. doi:10.1515/corrrev-2012-0502.

[15] E.G. Astafurova, E. V. Melnikov, S. V. Astafurov, I. V. Ratochka, I.P. Mishin, G.G. Maier, et al., Hydrogen Embrittlement of Austenitic Stainless Steels with Ultrafine-Grained Structures of Different Morphologies, Phys. Mesomech. 22 (2019) 313–326. doi:10.1134/s1029959919040076.

[16] E.D. Merson, P.N. Myagkikh, G. V. Klevtsov, D.L. Merson, A. Vinogradov, Effect of equal-channel angular pressing (ECAP) and current density of cathodic hydrogen charging on hydrogen trapping in the low-alloy steel, Lett. Mater. (2020) In press.

[17] G.I. Raab, R.Z. Valiev, D. V. Gunderov, T.C. Lowe, A. Misra, Y.T. Zhu, Long-length ultrafine-grained titanium rods produced by ECAP- conform, Mater. Sci. Forum. 584-586 PA (2008) 80–85. doi:10.4028/www.scientific.net/msf.584-586.80.

[18] E.D. Merson, P.N. Myagkikh, V.A. Poluyanov, D.L. Merson, A. Vinogradov, Quasi-cleavage hydrogen-assisted cracking path investigation by fractographic and side surface observations, Eng. Fract. Mech. 214 (2019) 177–193. doi:10.1016/j.engfracmech.2019.04.042.

[19] E.D. Merson, V.A. Poluyanov, D.L. Merson, A.Y. Vinogradov, About the Nature of Quasi-Cleavage in Low-Carbon Steel Embrittled with Hydrogen, Met. Sci. Heat Treat. 61 (2019) 191–195. doi:10.1007/s11041-019-00399-x.

[20] E. Merson, A.V. Kudrya, V.A. Trachenko, D. Merson, V. Danilov, A. Vinogradov, Quantitative characterisation of cleavage and hydrogen-assisted quasi-cleavage fracture surfaces with the use of confocal laser scanning microscopy, Mater. Sci. Eng. A. 665 (2016) 35–46. doi:10.1016/j.msea.2016.04.023.

[21] E. Merson, A. Vinogradov, D.L. Merson, Application of acoustic emission method for investigation of hydrogen embrittlement mechanism in the low-carbon steel, J. Alloys Compd. 645 (2015) S460–S463. doi:10.1016/j.jallcom.2014.12.083.